APPLIED PHYSICS

Long-term data storage in diamond

Siddharth Dhomkar,[1]* Jacob Henshaw,[1,2]* Harishankar Jayakumar,[1] Carlos A. Meriles[1,2]†

2016 © The Authors, some rights reserved; exclusive licensee American Association for the Advancement of Science. Distributed under a Creative Commons Attribution NonCommercial License 4.0 (CC BY-NC).

The negatively charged nitrogen vacancy (NV^-) center in diamond is the focus of widespread attention for applications ranging from quantum information processing to nanoscale metrology. Although most work so far has focused on the NV^- optical and spin properties, control of the charge state promises complementary opportunities. One intriguing possibility is the long-term storage of information, a notion we hereby introduce using NV-rich, type 1b diamond. As a proof of principle, we use multicolor optical microscopy to read, write, and reset arbitrary data sets with two-dimensional (2D) binary bit density comparable to present digital-video-disk (DVD) technology. Leveraging on the singular dynamics of NV^- ionization, we encode information on different planes of the diamond crystal with no cross-talk, hence extending the storage capacity to three dimensions. Furthermore, we correlate the center's charge state and the nuclear spin polarization of the nitrogen host and show that the latter is robust to a cycle of NV^- ionization and recharge. In combination with super-resolution microscopy techniques, these observations provide a route toward subdiffraction NV charge control, a regime where the storage capacity could exceed present technologies.

INTRODUCTION

Diamond is a unique platform material whose extreme properties and multifunctionalities are enabling an ever-growing set of applications ranging from the fabrication of long-lasting machining and cutting tools, to biomedical and low-wear coatings, and to efficient heat sinks for high-power electronics. Diamond typically contains impurities and other defects whose varying concentration and composition give gems their signature colors. An example of emerging importance is the negatively charged nitrogen vacancy (NV^-) center, a spin 1 complex formed by a substitutional nitrogen atom adjacent to a vacant site. These paramagnetic centers can be located individually using confocal microscopy, initialized via optical pumping, and read out through spin-dependent photoluminescence measurements (*1*). Optical access coupled to a single electron spin control and millisecond-long coherence spin lifetimes under ambient conditions (*2*) has led to recent demonstrations of entanglement and basic quantum logic (*3*–*7*), as well as various forms of nanoscale sensing (*8*–*11*).

Here, we use multicolor optical microscopy to locally convert the charge state of NVs within a dense ensemble from negative to neutral and correspondingly alter the NV fluorescence emission from bright to dark. This change is reversible, long-lasting, and robust to weak illumination, thus serving as an alternate platform for 3D information storage. To demonstrate this notion, we write, read, erase, and rewrite data, which, in this study, take the form of stacked two-dimensional images. Although presently limited by light diffraction, access to the NV electron and nuclear spin degrees of freedom could be potentially exploited to reduce the volume per bit. As a first step in this direction, we use a charge-to-spin (CTS) conversion protocol to polarize the nuclear spin of the nitrogen host, conditional on the NV charge state, and subsequently show that this polarization remains virtually unchanged throughout a cycle of NV^- ionization and recharge.

RESULTS

Storing and retrieving arbitrary data sets in three dimensions

The physical mechanisms underlying NV charge dynamics are presented in Fig. 1A: green illumination (for example, at 532 nm) ionizes an NV^- via the consecutive absorption of two photons, thus transforming the NV^- into an NV^0 (that is, a neutrally charged NV). Conversely, green light can drive a neutral NV into its excited state where absorption of an electron from the valence band reconverts NV^0 back into NV^- (Fig. 1A). Therefore, an NV center exposed to green light dynamically alters its charge state at a rate that depends on the illumination intensity (*12*, *13*). This behavior changes with the use of red light (for example, 632 nm), because photons of this wavelength can only excite NV^- but not NV^0. Consequently, strong red illumination ionizes NV^- to produce NV^0, but the back-conversion process is largely inhibited.

In our experiments, we used a type 1b diamond crystal with an approximate NV concentration of 0.4 parts per million (ppm). Two intuitive forms of charge patterning are presented in Fig. 1B: upon initializing the focal plane into NV^- (upper row), we convert select portions into NV^0 by successively parking a strong red beam at the desired pixels for a predefined time interval. Given the near quadratic dependence of the ionization rate on the illumination intensity (*13*), the resulting NV charge map can be revealed via a weak red laser scan. In this regime, charge ionization during readout is minimal, and the fluorescence—brighter in NV^--rich areas—correlates with NV^- concentration. The lower row in Fig. 1B illustrates the converse approach where patterning is attained by parking a green beam on a "bleached" (that is, NV^--deprived) plane. Exposure to green light locally reconverts NV^0 into NV^-, and subsequent fluorescence imaging—via a weak red scan—unveils the expected bright pattern on an otherwise dark background.

Both encoding protocols yield comparable pixel definition (about 0.8 μm; defined here by a numerical aperture of 0.42 of the objective; see fig. S1). However, green or red imprints respond differently to multiple red laser readouts (middle and left columns in Fig. 1B). Both exhibit a gradual loss of contrast, but the impact is substantially stronger on the green imprint. Remarkably, observations on test patterns over a period of a week show no noticeable change, provided that the diamond crystal is kept in the dark. Thus, data storage in diamond must be viewed as semipermanent in the sense that a "refresh" protocol is required, conditional on the number of readouts but independent on the total elapsed time.

To derive a more quantitative metric, we compare the fluorescence response from an arbitrary (but fixed) site of the diamond crystal to multiple readouts (fig. S2). We find not only that red imprinting features a slower fluorescence decay but also that the relative contrast

[1]Department of Physics, City University of New York (CUNY)–City College of New York, New York, NY 10031, USA. [2]CUNY–Graduate Center, New York, NY 10016, USA.
*These authors contributed equally to this work.
†Corresponding author. Email: cmeriles@ccny.cuny.edu

Downloaded from http://advances.sciencemag.org/ on August 9, 2018

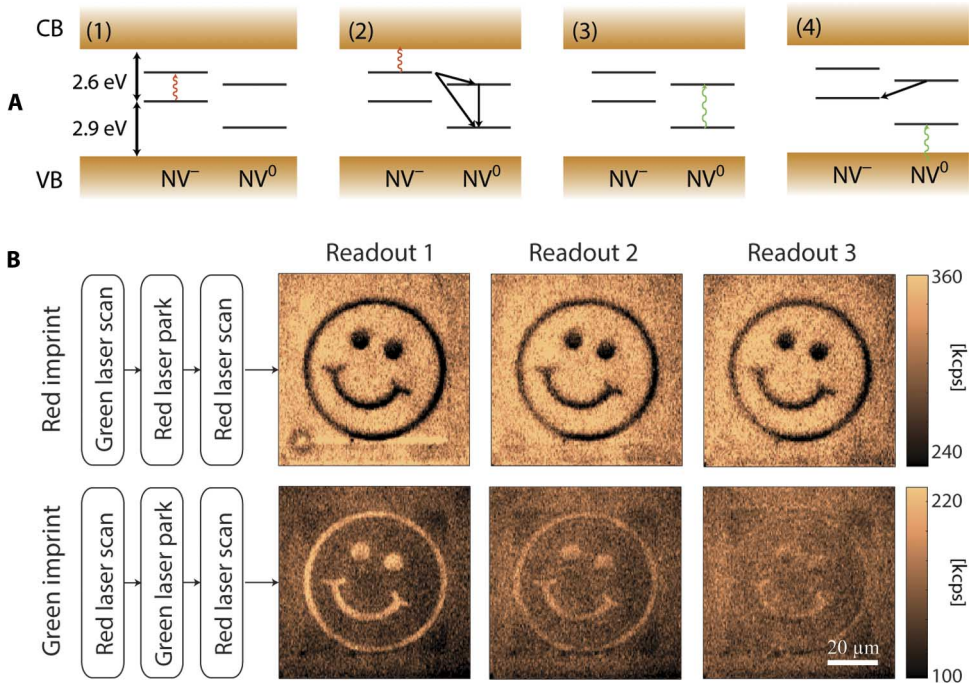

Fig. 1. Charge manipulation and readout in diamond. (**A**) Energy diagram for NV^- and NV^0. In (1) and (2), the successive absorption of two photons (wavy arrows) of energy equal or greater than 1.95 eV (637 nm) propels the excess electron of an NV^- into the conduction band, leaving the defect in the neutral ground state (solid arrows). In (3) and (4), an NV^0 consecutively absorbs two photons of energy equal or greater than 2.16 eV (575 nm) transforming into NV^-. CB, conduction band; VB, valence bands. (**B**) Top: A binary pattern on an NV^--rich background is imprinted via spatially selective red illumination (632 nm, 350 μW, 100 ms per pixel). Bottom: Starting from an NV^--depleted background, the pattern results from selective illumination with green laser light (532 nm, 30 μW, 5 ms per pixel). From left to right, images are the result of three successive readouts of the same original imprint via a red scan (200 and 150 μW for the upper and lower rows, respectively). In all cases, the image size is 100 × 100 pixels, and the integration time is 1 ms per pixel. kcps, kilocounts/s.

between "bright" and "dark" remains high over tens of readouts. This is not the case for a green imprint where the contrast first vanishes and then inverts. The physics at play is complex, and more investigation will be needed to gain a fuller understanding. However, initial work (*14*) indicates that the local N^+ content—higher when green light is present during the encoding process—plays an important role.

Unlike photorefractive polymers (which are prone to degradation upon repeated light exposure) (*15*) or gold nanorods (which undergo a permanent photoinduced shape change) (*16*, *17*), the charge state of the NV center can be reversibly altered with no accumulated effect, hence allowing one to erase and rewrite information a virtually limitless number of times. A proof-of-principle demonstration is presented in Fig. 2A (see also fig. S3): after resetting the NV^- content via a strong green laser scan (step 1), we proceeded to write the focal plane through a red imprint, which we then exposed via a weak red scan (step 2); the same protocol was then repeated to encode and read out a new, different pattern (steps 3 and 4). Note that unlike Fig. 1—where the brightness in each pixel takes one of two possible values—the images in Fig. 2A are imprinted using a variable exposure time per pixel. In the present case, we bin the illumination times into five different durations, which correspondingly lead to discernible levels of fluorescence, that is, the equivalent of a multivalued bit (fig. S1). The result is a concomitant boost of the information density, illustrated here via the grayscale images. The number of levels is largely defined by the signal-to-noise ratio (SNR) of the optical detection, which, in turn, grows with the square root of the readout time and NV density. In practice, considerations such as background noise and sample homogeneity must also be taken into account. For the conditions herein, up to eight different levels seem realistic (see fig. S1), although more are conceivable, for example, if the sample is engineered to host a higher NV concentration.

Because the illumination intensity decays with the inverse square of the distance to the focal plane, it is possible to selectively imprint the diamond at a given depth without altering the information stored elsewhere. A demonstration is presented in Fig. 2B, where we write NV charge maps on three stacked planes approximately 90 μm apart from each other. Given the thickness of the diamond sample we used (200 μm), these results indicate minimal optical aberrations throughout the crystal. On the other hand, the separation between planes—largely defined by the beam shape near the focal plane—could be reduced by resorting to beam-shaping techniques. In particular, a spatial light modulator could be used to adjust the optical wave front to reduce axial elongation in the beam profile.

Ultimately, the interplane separation results from a tradeoff between various parameters, including the required level of contrast, writing speed, and light intensity. For example, better in-plane localization is attained in the limit of low laser power, where the NV ionization rate responds quadratically to the illumination intensity (*13*), but the encoding time per pixel is comparatively longer. Faster writing speed can be reached with stronger laser power, but saturation of the first excited state gradually makes the NV ionization rate transition from quadratically to linearly dependent on the intensity, with the corresponding reduction of the in-plane localization (*12*). For a given laser power, a similar consideration applies to the light exposure time and fluorescence contrast, the latter improving with longer imprint times at the expense of a larger pixel volume (see also fig. S1). Note, however, that this tradeoff has a lesser impact on data density if the brighter fluorescence of larger pixels is

Downloaded from http://advances.sciencemag.org/ on August 9, 2018

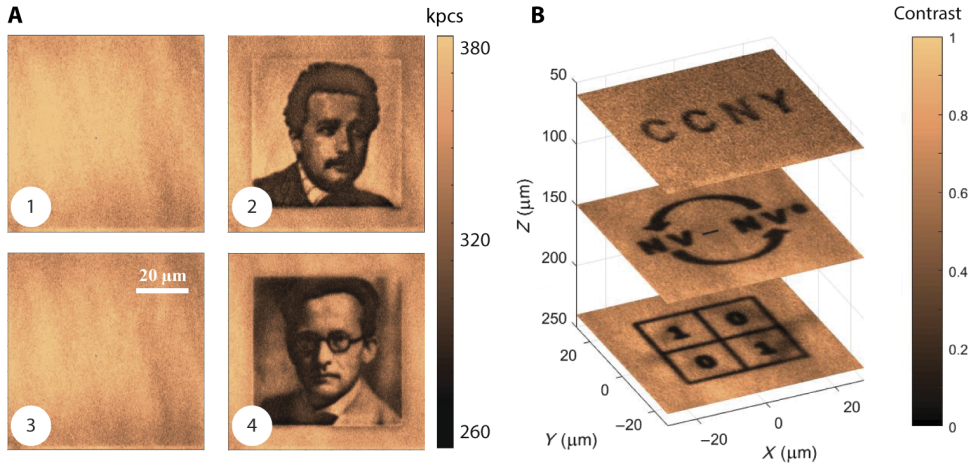

Fig. 2. Diamond as a 3D read/write memory. (**A**) Starting from a blank ensemble of NV^- centers (1), information can be written (2), erased (3), and rewritten (4). In (1) and (3), a green laser scan (1 mW at 1 ms per pixel) was used to reset the target plane to a bright state. In (2) and (4), images were imprinted via a red laser scan with a variable exposure time per pixel (from 0 to 50 ms). Note the gray scale in the resulting images corresponding to multivalued (as opposed to binary) encoding. The same scale bar applies to all four images. (**B**) Information can be stored and accessed in three dimensions, as demonstrated for the case of a three-level stack. Observations over a period of a week show no noticeable change in these patterns for a sample kept in the dark. In (A) and (B), readout is carried out via a red laser scan (200 μW at 1 ms per pixel). The image size is 150 × 150 pixels in all cases.

binned into discrete levels to produce multivalued bits, as discussed above (Fig. 2A).

The absolute write and read times per pixel—either comparable to or greater than 1 ms—presently make NV storage comparatively slow for practical applications, although there seems to be considerable room for improvement. The most obvious route to faster writing makes use of stronger illumination intensities, though at the expense of higher power consumption and system complexity. For a constant average laser power, pulsed excitation may prove beneficial given the quadratic response of NV ionization upon green or red illumination. Along the same lines, different excitation colors can markedly exhibit different ionization efficiencies (for example, see conditions in Fig. 1 for red and green imprinting), thus calling for systematic characterization as a function of the excitation wavelength. In particular, we show below that NV^- can be efficiently ionized by blue illumination (directly exciting the excess electron into the conduction band), although further work will be needed for a vis-à-vis comparison between one- and two-photon ionization in type 1b diamond. Although some of the same considerations also affect readout speed, the latter is mainly defined by SNR limitations, which, perhaps, could be ameliorated by increasing the NV content.

Toward super-resolution data storage

Whereas the spatial resolution of a diamond memory—or for that matter, any other optical memory (*15*–*18*)—is inherently influenced by light diffraction, a question of interest is whether the latter sets a fundamental limit to manipulate the NV charge. Super-resolution methods have already been applied to image NV centers with a spatial accuracy of up to ~6 nm (*19*), approximately 100th of the excitation wavelength. However, storing and accessing information with subdiffraction discrimination would require that the NV charge state be preserved during the write and readout processes, a condition difficult to meet with existing super-resolution imaging methods. This incompatibility is apparent in schemes such as stochastic optical reconstruction microscopy (*20*) or photoactivated localization microscopy (*21*), where spatial resolution is attained by randomly activating a small fraction of fluorophores while most of the ensemble remains in the dark state (*22*).

Subdiffraction imaging strategies that deterministically drive NVs into a nonfluorescing state are not exempt from problems. For example, in charge state depletion (CSD) microscopy (*23*), fluorescence is recorded using weak, nonionizing illumination following the successive application of a green Gaussian beam and a concentric, doughnut-shaped red beam. The former brings most NVs within the focal area into the bright, negatively charged state, whereas the latter selectively transforms peripheral NVs into the dark, neutrally charged state. Therefore, CSD microscopy is unsuited for high-density, subdiffraction recording because any given "write" operation initializes the charge state of NVs proximal to the target. This same drawback also applies to stimulated emission depletion (STED) microscopy (*19*) and related techniques (*24*, *25*) because uncontrolled NV ionization is at least as likely as stimulated emission during the application of the strong STED beam.

The ability to manipulate the NV spin degrees of freedom provides a versatile route to circumvent these problems. For example, because nuclear spins are relatively well isolated, the data loss during a super-resolution read/write could be eluded via the use of a CTS conversion scheme, where the nuclear spins of all NVs within the laser focal spot are polarized, conditional on the initial NV charge state. This route exploits the NV nuclear spins as ancillary memories to temporarily store the initial charge state of all illuminated NVs during a laser read/write. Using a doughnut beam to separately address the group of NVs surrounding the target, the original charge state can be subsequently reestablished via spin-to-charge (STC) conversion (*26*). Here, we are assuming that the experimental conditions are chosen so that the full protocol—including CTS, target read/write, and STC—takes place on a time scale shorter than the spin lattice relaxation time of the NV nuclear host.

An initial proof of concept containing key ingredients necessary for the realization of the above approach is presented in Fig. 3: upon preparing the NVs into the negatively charged state, we use an optical pumping scheme (*27*) to initialize the ^{14}N spin of the host nitrogen atom—a system

Downloaded from http://advances.sciencemag.org/ on August 9, 2018

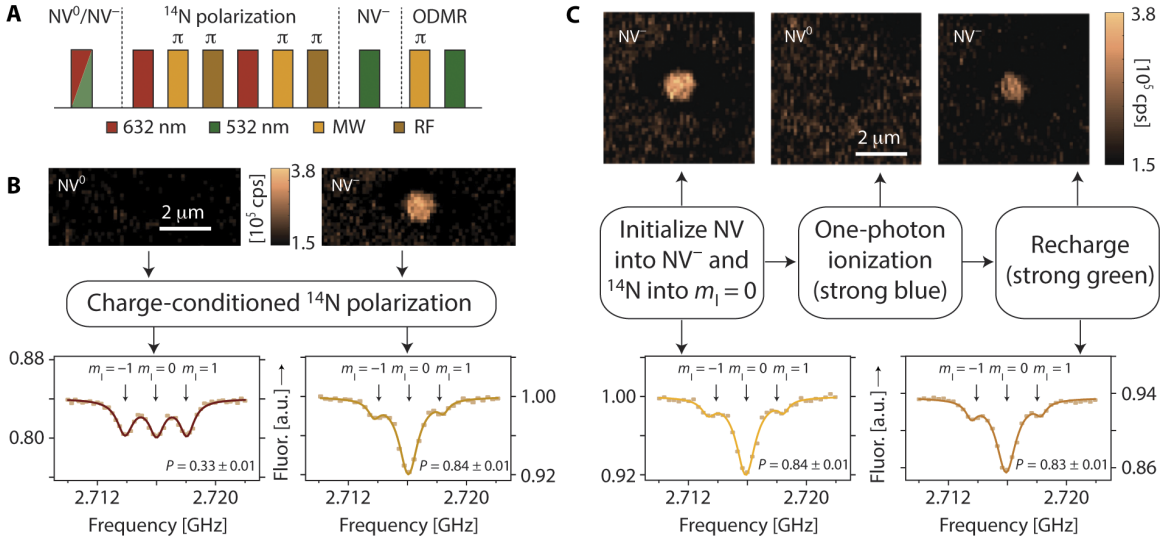

Fig. 3. Combined NV charge and spin manipulation. (**A**) Charge-conditional initialization of the ^{14}N nuclear spin host into $m_I = 0$ is attained via spin transfer from the optically polarized NV^- electronic spin (see also figs. S4 and S5). Initialization into NV^- (NV^0) is attained by applying (or not) a green laser pulse (532 nm, 1 mW, 10 μs) on an NV^--depleted background (632 nm, 250 μW, 50 ms per pixel). Following ^{14}N polarization, (unconditional) reconversion into NV^- is attained via a green laser pulse (532 nm, 1 mW, 3 μs). The durations of the MW and RF pulses are 440 ns and 28 μs, respectively. (**B**) Measured NV^- ODMR spectra after the application of the pulse sequence in (A). The upper images (632 nm, 250 μW, 1 ms per pixel) show the NV^- fluorescence in a vicinity of the probed sample spot (coincident with the image center) after charge initialization. (**C**) With the ^{14}N spin in the $m_I = 0$ state, negatively charged NVs undergo a cycle of ionization and recharge. The pulse protocol is identical to that in (A) except that a blue laser pulse (450 nm, 400 μW, 30 μs) is introduced after nuclear spin polarization, temporarily converting NV^- into NV^0, as indicated by the upper fluorescence images. Comparison of the ODMR spectra before (left) and after (right) the application of the ionization/recharge cycle nearly shows no change of the ^{14}N spin polarization. In (B) and (C), every point in the ODMR spectra corresponds to 10^5 consecutive averages; solid lines are Lorentzian fits to the three ^{14}N hyperfine peaks; *P* denotes the fractional area under the central peak. a.u., arbitrary units.

of spin number $I = 1$—into $m_I = 0$ (where m_I denotes the nuclear spin quantum projection along a direction coincident with the NV axis). This scheme uses a train of laser, microwave (MW), and radio frequency (RF) pulses to drive the ^{14}N spin into the desired final state (Fig. 3A and section S1). Optically detected magnetic resonance (ODMR) of the NV^- electronic spin (right column in Fig. 3B) reveals a hyperfine-split spectrum with a prominent central peak surrounded by two weak satellites, from where we estimate the level of nuclear spin polarization at about 80%.

Because both the electronic and spin energy levels depend on the center's charge state, the spin pumping protocol has no impact on the nuclear spins of neutral NVs, which consequently remain unpolarized. This charge selectivity is confirmed by interrogating NV centers initially prepared in the neutral state and subsequently converted to NV^- before ODMR inspection (left column in Fig. 3B); as expected, in this case, the spectrum displays three peaks of comparable amplitude, indicative of equal ^{14}N spin populations in all three projections. Conditional ^{14}N spin polarization thus amounts to "charge-to-spin" conversion, with fidelity ultimately limited by the chosen nuclear spin initialization protocol.

To recreate the impact of super-resolution schemes on the charge state of NVs near the target, we impose a cycle of forced ionization and recharge (Fig. 3C and section S2). Departing from the experiments illustrated in Figs. 1 and 2, NV^- ionization is carried out this time with the aid of a femtosecond laser tuned to emit at 450 nm. Unlike red or green illumination—in which the NV undergoes a two-step process (Fig. 1A)—one-photon excitation in the blue illumination directly propels the NV^- excess electron into the conduction band, hence avoiding light-induced nuclear spin depolarization via level mixing in the first excited state (*28*). To recharge NV^0, we used a strong green laser pulse whose duration is optimized to yield one-directional charge conversion into the NV^- state with minimum ^{14}N spin depolarization. Comparison of the ODMR spectra before and after the ionization-and-recharge cycle (lower left and right plots in Fig. 3C, respectively) virtually shows no change in the ^{14}N spin polarization, which demonstrates data protection against photoinduced charge conversion (see also figs. S4 and S5).

DISCUSSION

Further work will be necessary to gain charge control of individual or small groups of NVs with subdiffraction resolution, starting with the implementation of more efficient CTS conversion protocols, which are limited in this case by the fidelity of the chosen nuclear spin polarization scheme. Although the present experiments are carried out at only ~5.5 mT, greater nuclear spin resilience to photoionization is possible at higher magnetic fields (>200 mT), where state mixing–driven nuclear spin relaxation in the excited state is significantly reduced (*29*). By the same token, greater nuclear spin polarization contrast between neutral and negative NVs is feasible if the CTS protocol is improved so as to polarize complementary nuclear spin projections depending on the original charge state (for example, $m_I = -1$ for NV^- and $m_I = +1$ for NV^0).

Similar considerations apply to the converse operation, namely, the "spin-to-charge" transformation presently attainable at only moderate fidelities (*26*). Given the high spin selectivity of the intersystem crossing at room temperature, more efficient STC conversion is conceivable if the existing protocol is modified so as to induce ionization by one-photon excitation from the ground singlet state. Alternatively, it may be possible to exploit the longer electronic state lifetimes of NVs at low temperatures, though at the expense of a more complex experimental setup.

Downloaded from http://advances.sciencemag.org/ on August 9, 2018

By circumventing the limitations inherent to a storage medium that is confined to two dimensions (*30*, *31*), the ideas discussed herein can be extended to include other defects also acting as electron traps. These centers could be exploited, for example, for error correction so as to mitigate charge instabilities from electron tunneling between neighboring NV centers or between NV centers and surrounding substitutional nitrogen atoms [most likely in crystals with high NV and nitrogen concentration (*32*)]. By the same token, material platforms other than NVs in diamond may also be exploited for high-density data storage; examples include the silicon-carbon divacancy (*33*) and the silicon vacancy (*34*) in SiC as well as select rare earth ions in garnets (*35*), all of which exhibit controllable charge and electronic/nuclear spin degrees of freedom.

MATERIALS AND METHODS

Diamond crystal

A type 1b [111] diamond from Diamond Delaware Knives was used as the sample. Prior characterization via infrared spectroscopy (*14*) was consistent with the presence of substitutional nitrogen atoms at a concentration of approximately 40 ppm; the estimated NV content was 0.4 ppm. The absorption near 1282 cm^{-1} suggests that A-centers—formed by two adjacent nitrogen atoms—were, if at all present, at trace concentrations. Optical spectroscopy confirms that the collected fluorescence originated almost exclusively from NV centers. A distinctive peak at ~737 nm reveals the presence of silicon vacancy (SiV) centers; from the peak amplitude, we estimated the SiV-NV ratio to be about 0.6%.

NV magnetic resonance and optical microscopy

For our experiments, we used a custom-made, multicolor microscope. A 13-mW helium-neon laser and a 2 W continuous-wave solid-state laser served as the sources of red (632 nm) and green (532 nm) light, respectively. Excitation in the blue (450 nm) light was provided by a tunable ultrafast laser (Coherent Mira) and a frequency doubler generating 120-fs-long pulses at a repetition rate of 76 MHz; the average power at 450 nm was 400 μW. All laser beams were coupled into a 0.42–numerical aperture objective, which also collected the outgoing sample fluorescence. The illumination timing was set independently with the aid of acousto-optic modulators; a servo-controlled, two-mirror galvo system was used for sample scanning. Sample fluorescence ranging from 650 to 850 nm was detected after a dichroic mirror and notch filters by a solid-state avalanche photodetector.

Control of the NV^- electronic and nuclear spin was carried out via the use of MW and RF pulses produced by four signal generators: R&S SMB100A, R&S SMV03, Agilent E4433B, and Tektronix AFG3102. A 25-μm-diameter copper wire overlaid on the diamond surface served as the simultaneous source of the MW and RF fields. Upon amplification, the typical duration of an MW (RF) inversion pulse was 500 ns (30 μs). All magnetic resonance experiments were carried out in the presence of a 5.5-mT magnetic field emanating from a permanent magnet in the sample vicinity. The magnetic field was oriented so as to coincide with the sample crystal normal, that is, the [111] axis. A pulse generator (PulseBlasterESR-PRO) controlled the timing of all laser, MW, and RF pulses. All experiments were carried out under ambient conditions.

SUPPLEMENTARY MATERIALS

Supplementary material for this article is available at http://advances.sciencemag.org/cgi/content/full/2/10/e1600911/DC1

section S1. Charge-conditioned polarization of the ^{14}N spin.
section S2. Impact of NV^- ionization and recharge on the ^{14}N spin polarization.
fig. S1. Spatial resolution of NV charge patterning.
fig. S2. Impact of multiple readouts on NV fluorescence contrast.
fig. S3. NV response upon multiple read/write cycles.
fig. S4. Impact of NV^- ionization on the ^{14}N nuclear spin polarization.
fig. S5. Impact of NV^- recharge on the ^{14}N nuclear spin polarization.

REFERENCES AND NOTES

1. F. Jelezko, T. Gaebel, I. Popa, A. Gruber, J. Wrachtrup, Observation of coherent oscillations in a single electron spin. *Phys. Rev. Lett.* **92**, 076401 (2004).
2. G. Balasubramanian, P. Neumann, D. Twitchen, M. Markham, R. Kolesov, N. Mizuochi, J. Isoya, J. Achard, J. Beck, J. Tissler, V. Jacques, P. Hemmer, F. Jelezko,J. Wrachtrup, Ultralong spin coherence time in isotopically engineered diamond. *Nat. Mater.* **8**, 383–387 (2009).
3. M. V. Gurudev Dutt, L. Childress, L. Jiang, E. Togan, J. Maze, F. Jelezko, A. S. Zibrov, P. R. Hemmer, M. D. Lukin, Quantum register based on individual electronic and nuclear spin qubits in diamond. *Science* **316**, 1312–1316 (2007).
4. P. Neumann, N. Mizuochi, F. Rempp, P. Hemmer, H. Watanabe, S. Yamasaki, V. Jacques, T. Gaebel, F. Jelezko, J. Wrachtrup, Multipartite entanglement among single spins in diamond. *Science* **320**, 1326–1329 (2008).
5. P. Neumann, R. Kolesov, B. Naydenov, J. Beck, F. Rempp, M. Steiner, V. Jacques, G. Balasubramanian, M. L. Markham, D. J. Twitchen, S. Pezzagna, J. Meijer, J. Twamley, F. Jelezko, J. Wrachtrup, Quantum register based on coupled electron spins in a room-temperature solid. *Nat. Phys.* **6**, 249–253 (2010).
6. P. C. Maurer, G. Kucsko, C. Latta, L. Jiang, N. Y. Yao, S. D. Bennett, F. Pastawski, D. Hunger, N. Chisholm, M. Markham, D. J. Twitchen, J. I. Cirac, M. D. Lukin, Room-temperature quantum bit memory exceeding one second. *Science* **336**, 1283–1286 (2012).
7. E. Togan, Y. Chu, A. S. Trifonov, L. Jiang, J. Maze, L. Childress, M. V. G. Dutt, A. S. Sørensen, P. R. Hemmer, A. S. Zibrov, M. D. Lukin, Quantum entanglement between an optical photon and a solid-state spin qubit. *Nature* **466**, 730–734 (2010).
8. T. Staudacher, F. Shi, S. Pezzagna, J. Meijer, J. Du, C. A. Meriles, F. Reinhard, J. Wrachtrup, Nuclear magnetic resonance spectroscopy on a (5-nanometer)^3 sample volume. *Science* **339**, 561–563 (2013).
9. H. J. Mamin, M. Kim, M. H. Sherwood, C. T. Rettner, K. Ohno, D. D. Awschalom, D. Rugar, Nanoscale nuclear magnetic resonance with a nitrogen-vacancy spin sensor. *Science* **339**, 557–560 (2013).
10. T. Häberle, D. Schmid-Lorch, F. Reinhard, J. Wrachtrup, Nanoscale nuclear magnetic imaging with chemical contrast. *Nat. Nanotechnol.* **10**, 125–128 (2015).
11. T. M. Staudacher, N. Raatz, S. Pezzagna, J. Meijer, F. Reinhard, C. A. Meriles, J. Wrachtrup, Probing molecular dynamics at the nanoscale via an individual paramagnetic center. *Nat. Commun.* **6**, 8527 (2015).
12. G. Waldherr, J. Beck, M. Steiner, P. Neumann, A. Gali, T. Frauenheim, F. Jelezko, J. Wrachtrup, Dark states of single nitrogen-vacancy centers in diamond unraveled by single shot NMR. *Phys. Rev. Lett.* **106**, 157601 (2011).
13. N. Aslam, G. Waldherr, P. Neumann, F. Jelezko, J. Wrachtrup, Photo-induced ionization dynamics of the nitrogen vacancy defect in diamond investigated by single-shot charge state detection. *New J. Phys.* **15**, 013064 (2013).
14. H. Jayakumar, J. Henshaw, S. Dhomkar, D. Pagliero, A. Laraoui, N. B. Manson, R. Albu, M. W. Doherty, C. A. Meriles, Optical patterning of trapped charge in nitrogen-doped diamond. *Nat. Commun.* **7**, 12660 (2016).
15. D. Day, M. Gu, A. Smallridge, Use of two-photon excitation for erasable-rewritable three-dimensional bit optical data storage in a photo refractive polymer. *Opt. Lett.* **24**, 948–950 (1999).
16. P. Zijlstra, J. W. M. Chon, M. Gu, Five-dimensional optical recording mediated by surface plasmons in gold nano rods. *Nature* **459**, 410–413 (2009).
17. Z. Gan, Y. Cao, R. A. Evans, M. Gu, Three-dimensional deep sub-diffraction optical beam lithography with 9 nm feature size. *Nat. Commun.* **4**, 2061 (2013).
18. M. Gu, X. Li, Y. Cao, Optical storage arrays: A perspective for future big data storage. *Light Sci. Appl.* **3**, e177 (2014).
19. E. Rittweger, K. Young Han, S. E. Irvine, C. Eggeling, S. W. Hell, STED microscopy reveals crystal colour centres with nanometric resolution. *Nat. Photonics* **3**, 144–147 (2009).
20. M. J. Rust, M. Bates, X. Zhuang, Sub-diffraction-limit imaging by stochastic optical reconstruction microscopy (STORM). *Nat. Methods* **3**, 793–795 (2006).
21. E. Betzig, G. H. Patterson, R. Sougrat, O. W. Lindwasser, S. Olenych, J. S. Bonifacino, M. W. Davidson, J. Lippincott-Schwartz, H. F. Hess, Imaging intracellular fluorescent proteins at nanometer resolution. *Science* **313**, 1642–1645 (2006).
22. M. Pfender, N. Aslam, G. Waldherr, P. Neumann, J. Wrachtrup, Single-spin stochastic optical reconstruction microscopy. *Proc. Natl. Acad. Sci. U.S.A.* **111**, 14669–14674 (2014).
23. X. Chen, C. Zou, Z. Gong, C. Dong, G. Guo, F. Sun, Subdiffraction optical manipulation of the charge state of nitrogen vacancy center in diamond. *Light Sci. Appl.* **4**, e230 (2015).

Downloaded from http://advances.sciencemag.org/ on August 9, 2018

24. E. Rittweger, D. Wildanger, S. W. Hell, Far-field fluorescence nanoscopy of diamond color centers by ground state depletion. *Europhys. Lett.* **86**, 14001 (2009).
25. K. Y. Han, S. K. Kim, C. Eggeling, S. W. Hell, Metastable dark states enable ground state depletion microscopy of nitrogen vacancy centers in diamond with diffraction-unlimited resolution. *Nano Lett.* **10**, 3199–3203 (2010).
26. B. J. Shields, Q. P. Unterreithmeier, N. P. de Leon, H. Park, M. D. Lukin, Efficient readout of a single spin state in diamond via spin-to-charge conversion. *Phys. Rev. Lett.* **114**, 136402 (2015).
27. D. Pagliero, A. Laraoui, J. Henshaw, C. A. Meriles, Recursive polarization of nuclear spins in diamond at arbitrary magnetic fields. *Appl. Phys. Lett.* **105**, 242402 (2014).
28. L. Jiang, M. V. Gurudev Dutt, E. Togan, L. Childress, P. Cappellaro, J. M. Taylor, M. D. Lukin, Coherence of an optically illuminated single nuclear spin qubit. *Phys. Rev. Lett.* **100**, 073001 (2008).
29. P. Neumann, J. Beck, M. Steiner, F. Rempp, H. Fedder, P. R. Hemmer, J. Wrachtrup, F. Jelezko, Single-shot readout of a single nuclear spin. *Science* **329**, 542–544 (2010).
30. S. Loth, S. Baumann, C. P. Lutz, D. M. Eigler, A. J. Heinrich, Bistability in atomic-scale antiferromagnets. *Science* **335**, 196–199 (2012).
31. C. R. Moon, L. S. Mattos, B. K. Foster, G. Zeltzer, H. C. Manoharan, Quantum holographic encoding in a two-dimensional electron gas. *Nat. Nanotechnol.* **4**, 167–172 (2009).
32. N. Manson, J. Harrison, Photo-ionization of the nitrogen-vacancy center in diamond. *Diamond Relat. Mater.* **14**, 1705–1710 (2005).
33. W. F. Koehl, B. B. Buckley, F. J. Heremans, G. Calusine, D. D. Awschalom, Room temperature coherent control of defect spin qubits in silicon carbide. *Nature* **479**, 84–87 (2011).
34. M. Widmann, S.-Y. Lee, T. Rendler, N. T. Son, H. Fedder, S. Paik, L.-P. Yang, N. Zhao, S. Yang, I. Booker, A. Denisenko, M. Jamali, S. Ali Momenzadeh, I. Gerhardt, T. Ohshima, A. Gali, E. Janzén, J. Wrachtrup, Coherent control of single spins in silicon carbide at room temperature. *Nat. Mater.* **14**, 164–168 (2015).
35. R. Kolesov, K. Xia, R. Reuter, R. Stöhr, A. Zappe, J. Meijer, P. R. Hemmer, J. Wrachtrup, Optical detection of a single rare-earth ion in a crystal. *Nat. Commun.* **3**, 1029 (2012).

Acknowledgments: We thank D. Pagliero for assistance with some of the experiments. **Funding:** Support for this work was provided by NSF through grant NSF-1314205. **Author contributions:** S.D., J.H., and H.J. conducted the experiments. C.A.M. supervised the work and wrote the manuscript. All authors discussed the results. **Competing interests:** The authors declare that they have no competing interests. **Data and materials availability:** All data needed to evaluate the conclusions in the paper are present in the paper and/or the Supplementary Materials. Additional data related to this paper may be requested from the authors.

Submitted 27 April 2016
Accepted 27 September 2016
Published 26 October 2016
10.1126/sciadv.1600911

Citation: S. Dhomkar, J. Henshaw, H. Jayakumar, C. A. Meriles, Long-term data storage in diamond. *Sci. Adv.* **2**, e1600911 (2016).

Downloaded from http://advances.sciencemag.org/ on August 9, 2018

Science Advances

Long-term data storage in diamond

Siddharth Dhomkar, Jacob Henshaw, Harishankar Jayakumar and Carlos A. Meriles

Sci Adv **2** (10), e1600911.
DOI: 10.1126/sciadv.1600911

ARTICLE TOOLS http://advances.sciencemag.org/content/2/10/e1600911

SUPPLEMENTARY MATERIALS http://advances.sciencemag.org/content/suppl/2016/10/24/2.10.e1600911.DC1

REFERENCES This article cites 35 articles, 9 of which you can access for free
http://advances.sciencemag.org/content/2/10/e1600911#BIBL

PERMISSIONS http://www.sciencemag.org/help/reprints-and-permissions

Use of this article is subject to the Terms of Service

Science Advances (ISSN 2375-2548) is published by the American Association for the Advancement of Science, 1200 New York Avenue NW, Washington, DC 20005. 2017 © The Authors, some rights reserved; exclusive licensee American Association for the Advancement of Science. No claim to original U.S. Government Works. The title *Science Advances* is a registered trademark of AAAS.

Downloaded from http://advances.sciencemag.org/ on August 9, 2018